Evaluation of an improved vented deflagration CFD model against nine experimental cases

Tolias, I.C.[1], Venetsanos, A.G.[1], Kuznetsov, M.[2]

[1] Environmental Research Laboratory, INRASTES, National Centre for Scientific Research Demokritos, Patriarchou Grigoriou E & 27 Neapoleos Str., 15341, Agia Paraskevi, Greece, tolias@ipta.demokritos.gr

[2] Institute of Nuclear and Energy Technologies, Karlsruhe Institute of Technology, Hermann-von-Helmholtz-Platz 1, 76344, Eggenstein-Leopoldshafen, Germany, mike.kuznetsov@kit.edu

ABSTRACT

In the present work, a newly developed CFD deflagration model incorporated into the ADREA-HF code is evaluated against hydrogen vented deflagrations experiments carried out by KIT and FM-Global in a medium (1 m^3) and a real (63.7 m^3) scale enclosure respectively. A square vent of 0.5 m^2 and 5.4 m^2 respectively is located in the center of one of side walls. In the case of the medium scale enclosure the 18% v/v homogeneous hydrogen-air mixture and back-wall ignition case is examined. In the case of the real scale enclosure many cases are examined which cover different mixture concentrations (homogeneous 15% and 18% v/v), different ignition locations (back-wall and central) and different levels of initial turbulence. The CFD model accounts for flame instabilities that develop as the flame propagates inside the chamber and turbulence that mainly develops outside the vent. Pressure predictions are compared against experimental measurements revealing a very good performance of the CFD model for the back-wall ignition cases. For the central ignition cases, the model overestimates the maximum overpressure. The opening of the vent cover is identified as a possible reason for the overprediction. The analysis indicates that turbulence is the main factor which leads to the violent external explosion causing the sudden pressure increase, confirming previous findings.

1.0 INTRODUCTION

Hydrogen use is expected to increase in the near future and its explosive nature brings up significant safety issues. In the case of an accident, hydrogen mixes with air and forms a flammable cloud. An accidental release in closed space can have catastrophic consequences in the case of an explosion. The confined space will lead to the development of much higher over-pressure compared to a similar explosion in open space. The venting of the compartment is the final protection measure in order to mitigate the damages of the explosion. In the past years, the increase of computational power has rendered Computational Fluid Dynamics (CFD) as a very attractive methodology for risk assessment. With its high numerical accuracy, it can evaluate regulations and standards and give deeper insight into the physical phenomenon.

External explosion is a phenomenon of increased importance in vented geometers because it can significantly increase the internal pressure. As the combustion develops inside the enclosure, unburned mixture is pushed outside through the vent. When the flame exits the vent, the mixture outside starts burning creating a secondary explosion. This explosion seems to have much more strength than the internal one. The main reasons that have been proposed for that behavior are the creation of extensive turbulence in the area outside the vent because of the jet-like flow, and the development of Rayleigh-Taylor instability due to the acceleration of the light products through the vent to the dense unburned mixture. Both reasons potentially lead to an augmentation of the reaction rate which leads to a violent external explosion. The pressure increase in the area outside the vent causes the decrease of the venting rate and consequently the increase of the internal pressure. A recent analysis of the peak over-pressures in vented explosion has been made by Chao et al. [1], where the effects of fuel, enclosure size, ignition location, vent size and obstacles were examined. Special attention to external explosion has been paid in several works such as [2][3][4].

CFD modeling of deflagrations is a big challenge. Combustion occurs at very small scales of the order of millimeters whereas geometries of practice interest are of order of meters. The growth of instabilities at the flame front, the complex interaction between the flame and the turbulence along with the very wide range of applications, make the development of a global model a difficult task. External explosion introduce an addition difficulty in deflagration modelling. Molkov et al. [5][6] performed Large Eddy Simulation (LES) to model a large-scale explosion in a vented enclosure (10 x 8.75 x 6.25 m), revealing the issue of external explosion modeling. In order to reproduce the experimental results, the combustion rate needed to be increased by approximately a factor of 2 at the area outside the vent. A similar approach was followed by Makarov et al. [7] in vented explosion through relief pipe. Bauwens et al. [8] and Keenan et al. [9] simulated hydrogen deflagrations in a vented room (4.6 x 4.6 x 3.0 m) focusing on the modeling of Rayleigh-Taylor instability for the correct reproduction of external explosion. The instability was modelled through an additional transport equation which takes into account the generation and the suppression rate of the instability.

In the current work, nine hydrogen vented deflagration experimental cases are simulated using the CFD method. The primary objective is the accurate prediction of the overpressure until the time that external explosion occurs. Thus, we do not deal with modelling of flame-acoustic interactions that may enhance the combustion rate at later stages. A newly developed model is presented and evaluated against the experiments.

2.0 DESCRIPTION AND ANALYSIS OF EXPERIMENTS

In order to evaluate the new deflagration model, a hydrogen deflagration experiment performed by KIT in a medium scale enclosure [10][11] and vented deflagration experiments performed by FM-Global [8][12] in a large scale chamber are chosen. The description of the experiments and discussion on their results are presented in the following Sections 2.1 and 2.2.

2.1 KIT experiments

In KIT experiment [10][11], the facility consists of an empty enclosure of 0.98 x 0.96 x 1.0 m (length x width x height) with a vent 0.5 x 0.5 m in size located in the center of a front wall. The enclosure is positioned inside a room of 5.5 m x 8.5 m x 3.4 m. The walls of the room are covered with damping material and special corrugated metal sheets to absorb shock waves. The distance of the right room wall from the enclosure closest side is 1.94 m, of the left wall 2.6 m, of the back-wall 1.95 m and of the ground 0.62 m. Outside the vent a beam structure exists which holds the measurements devices. This structure is included in the simulations. The distance of the horizontal beam edge from the vent is set equal to 0.15 m. The mixture is ignited at the center of the opposite to the vent wall (back-wall ignition). In the experiments, a thin plastic film was used as hermetic cover for the vent during the filling procedure. It was removed prior to ignition to avoid any influence on the results.

The pressure was measured at several positions inside and outside the enclosure. Two positions will be used here to compare with the experiment, pressure P03 located inside the enclosure at the centre of its bottom side and pressure P09 located 0.24 m outside the vent at the centreline. Furthermore, visualization of the burned and the unburned mixture was made, using the BOS-schlieren technique. Thus the flame front shape can be compared with the simulation results.

Experiments with homogeneous 7, 10, 12, 15 and 18% hydrogen-air mixture were performed. The experiment with 18% hydrogen is simulated in the current study. This experiment was conducted four times under the same conditions in order to test repeatability. The code numbers of these experiments were HIWP3-028, HIWP3-029, HIWP3-030, HIWP3-031. In this study, for simplification, these names are referred as 028, 029, 030 and 031 respectively.

In Figure 1 (top) the internal and external overpressure time series are presented for each repetition of the experiment. We observe that the results of the experiments 029, 030, 031 are very similar with

each other, at least until the time of the main pressure peak which is the area of interest. The maximum (filtered) overpressure for those experiments lies between 12.05 and 13.17 kPa for the internal one and between 7.56 and 8.69 kPa for the external one.

Experiment 028 is the only one which differs noticeable from the rest. The differences, however, is only quantitative because all overpressure curves exhibit similar behaviour: As the flame propagates inside the enclosure the internal pressure gradually increases until the flame exits the vent at approximately 0.078 s for experiments 029-031 and 0.086 s for experiment 028 (photos of the flame at these times for experiments 030 and 028 are presented in Figure 1). The internal pressure remains steady for a small time interval in all experiments and then suddenly increases due to the external explosion, i.e. the combustion of the unburned fuel that has been pushed outside the vent. The sudden increase of the external pressure occurs at about 0.082 s and 0.089 s for experiment 028 and 030 respectively (photos of the flame at these times are presented in Figure 1). The reason for the quantitative differences of experiment 028 is not clear to the experimentalists. The propagation speed inside the enclosure is slower compared to the speed in the other experiments leading to a lower rate of pressure rise (mainly while the flame propagates inside the enclosure) and lower maximum overpressure peaks.

In the bottom of Figure 1 the internal and external overpressure curves are presented together for each experiment. We observe that the external explosion effect appears in all experiments. The overpressure inside the enclosure increases rapidly reaching the maximum value after the sudden increase of the external one. The external explosion effect is confirmed in the examination of the flame front position from the video recordings [10][11]. In these videos it is shown that unburned mixture is pushed outside the enclosure during the propagation of the flame inside the enclosure from the back-wall to the vent. Once the flame has exited the vent, this mixture is ignited leading to the external overpressure peak. We should note that, as it is clear from the flame photos in Figure 1, the sudden increase of the external pressure occurs at the later stage of the external explosion and not immediately after the exit of the flame from the vent.

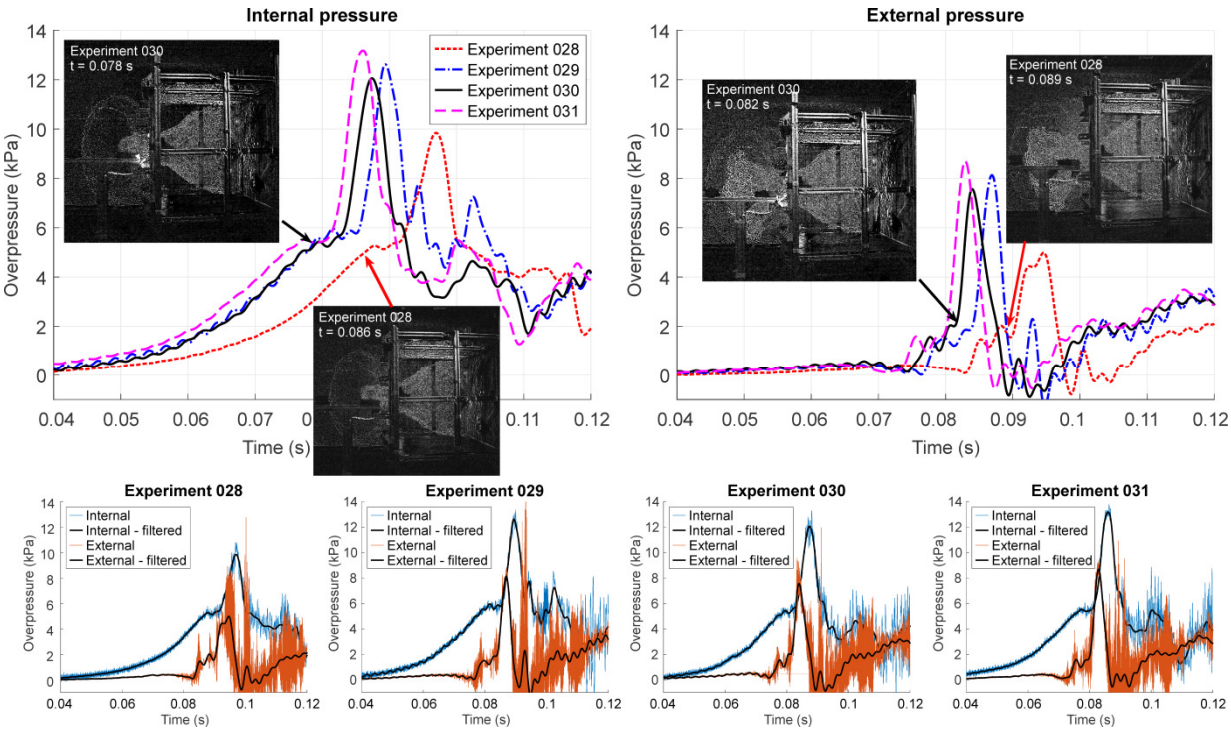

Figure 1. KIT experiments [10][11]. Top: Low pass filtered (400 Hz) internal and external pressure for the four repetitions of the experiment. Bottom: Internal and external pressure (filtered and unfiltered) in the same plot for each repetition of the experiment - the external explosion effect is depicted.

2.2 FM-Global experiments

A series of hydrogen vented deflagration experiments with various concentrations, vent openings and ignition locations were performed by FM-Global [8][12][13]. The experimental facility consists of a square-floored enclosure of 4.6 x 4.6 x 3.0 m (length x width x height) with a square vent. Eight cases are simulated in the current study with empty enclosure and vent area equal to 5.4 m^2.

In the first two cases, homogeneous 18% hydrogen-air mixture exists inside the enclosure which is ignited either near the back-wall or at the center of the enclosure. These experiments were initially conducted as it is descripted in [8][14][15]. In 2013, these experiments were repeated using a new chamber configuration [16]. In this configuration, the frame structure outside the chamber and the flame time of arrival thermocouples was removed, the ignition source was changed and the vent cover was perforated prior to the test. The last change seems to be the most important one because, in the new configuration, the vent cover is removed completely at very low overpressure (less than 0.5 kPa [12]). As a result, the effect on the results is smaller than in the initial configuration. The initial turbulent intensity is small, with u' being approximately equal to 0.1 m/s.

In Figure 2 the results of these two cases are presented for the old and the new configuration. The internal pressure was measured at four positions within the enclosure. The filtered pressure time-series was the same for all pressure sensors that were located away from the vent. The external pressure was measured on the concrete pad (at the same height as the bottom of the vent), 1.14 m away from the vent opening. We observe that the results from the different configurations have significant qualitative and quantitative differences. Qualitatively, in the new configuration a pressure drop occurs before the sudden increase of pressure at approximately 0.25 and 0.17 s for the back and center ignition case respectively. Moreover, in the center ignition case, the distinct second peak which is due to flame-acoustics interaction is almost vanished in the new configuration. Quantitatively, the pressure peak in the new configuration is bigger by approximately 28% in the back ignition case and smaller by approximately 19% in the center ignition case.

Consequently, the importance of minimizing the effect of the vent cover is depicted. Vent cover is difficult to be modeled with accuracy and thus experiments which minimize its impact on the results are necessary in order to increase the reliability of model validation.

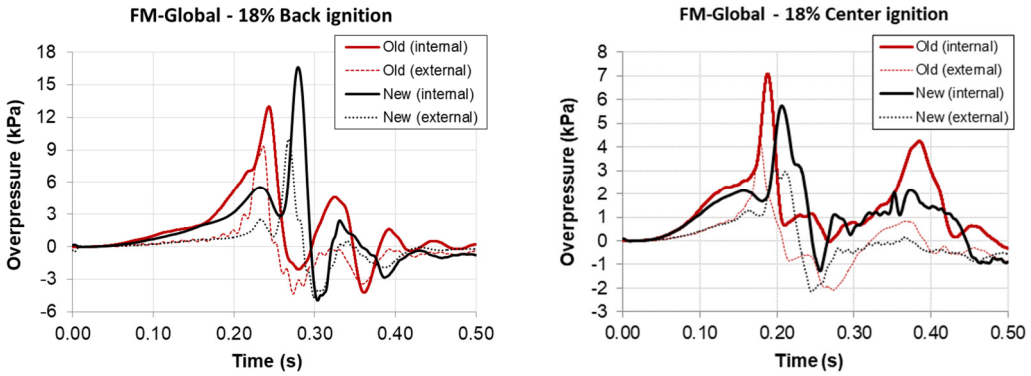

Figure 2. FM-Global experiments, 18% v/v hydrogen concentration [8][16]. Comparison of the overpressures time series for the new and old configuration for back (left) and center (right) ignition cases.

Comparing with the KIT case, we observe that the external explosion effect appears in FM-Global experiments too. The overpressure inside the enclosure increases rapidly reaching the maximum value after the sudden increase of the external one. This is obvious in both old and new configuration. On the other hand, the overpressure drop in internal pressure that is observed before the external explosion does not occur in KIT experiment in which the pressure remains constant. A possible reason for this difference could be the different vent coefficient ($K = V^{2/3}/A_v$ where V the volume of the enclosure

and A_v the area of the vent) of the two experiments. In KIT the vent coefficient is equal to 4 whereas in FM-Global is approximately equal to 3. Smaller vent coefficient means higher vent area and thus increased outflow which compensates the pressure increase. Regarding the maximum overpressure in back-wall experiments, its value between KIT and FM-Global is close due to the similar vent coefficient values.

In the other six experimental cases which are examined in the present study, the mixture composition is equal to 15% [12]. The vent cover was perforated prior to the test in these experiments too and a deployment pressure less than 0.5 kPa was measured. Three different initial level of turbulence (u' equal to 0.12, 0.40 and 0.50 m/s) and two ignition cases (back and center) are examined. The internal overpressure time series are presented in Figure 3. Similarly to the 18% cases (Figure 2), a pressure drop occurs before the sudden increase of pressure at approximately 0.35 and 0.28 s for the back and central ignition case respectively. We observe also that the increased levels of initial turbulence lead to greater overpressure peaks.

There are some significant differences between back and central ignition cases. The dependence of overpressure peaks on u' is not similar. The increase of u' from 0.4 to 0.5 m/s lead to 16% increase of the maximum overpressure in the back ignition case and to 41% increase in the central ignition case. The pressure signal for the center ignition case seems to be more "unstable" with more local maximum to occurs, especially in the cases of u' equal to 0.12 and 0.4 m/s. The vent cover opening may be responsible for these differences. Vent opening may have a greater influence in the center ignition case because the flame arrives earlier at the vent compared to the back ignition case. Vent opening seems to be evident in the overpressure time series in the center ignition case, because overpressure remains constant when the value of 0.5 kPa is reached (at about 0.16 s).

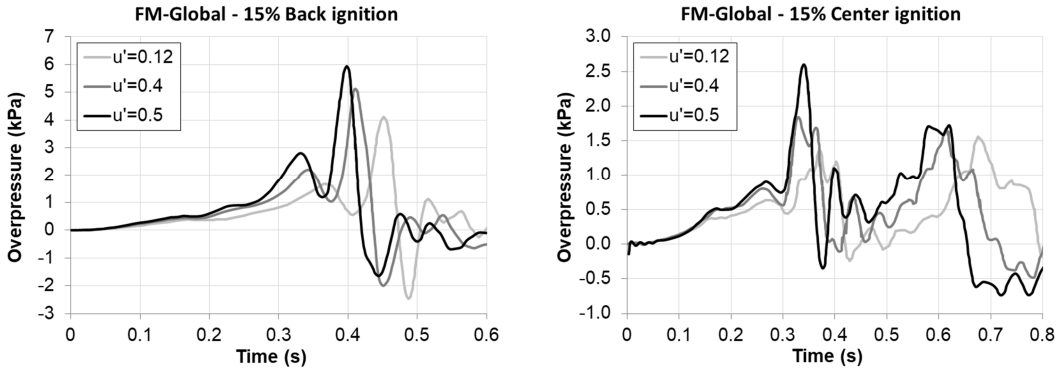

Figure 3. FM-Global experiments, 15% v/v hydrogen concentration [12]. Internal pressure time series for different levels of initial turbulence for back (left) and center (right) ignition cases.

3.0 NUMERICAL MODELLING

3.1 Governing equations - Combustion model

For the CFD simulations the ADREA_HF code was used [17][18]. The model solves the ensemble-averaged continuity equation, the Navier-Stokes equations, the energy equation (conservation equation of total enthalpy) and the conservation equation of hydrogen, oxygen and water mass fraction (one step irreversible reaction equation for hydrogen combustion is used). The multi-component mixture is assumed to be in thermodynamic equilibrium. The ideal gas equation of state is used. Turbulence is modelled using the URANS (Unsteady Reynolds averaged Navier-Stokes equations) approach and the Kato and Launder modification of the k-ε model was used [19].

The newly combustion model that we recently presented in [20] is used and is described briefly in next. The reaction rate for hydrogen which appears in its conservation equation is modelled based on the turbulent burning velocity (S_T) concept [21]:

$$\overline{R}_f = \rho_u S_T \left| \nabla q_f \right| \tag{1}$$

where q_f is the fuel mass fraction and ρ_u is the density in the unburned region which is estimated using the assumption of adiabatic compression. The turbulent burning velocity is modelled considering all the main factors that affect the total reaction rate: laminar burning velocity, turbulence existing in front of the flame front, hydrodynamic instability and non-equidiffusive effects. It is estimated from the relations:

$$S_T' = S_L + u'\left(1 + Da^{-2}\right)^{-1/4} \tag{2}$$

$$S_T = \Xi_k \cdot \Xi_{lp} \cdot \Xi_{T_0} \cdot S_T' \tag{3}$$

In these relations, S_T is the turbulent burning velocity, S_T' the intermediate turbulent burning velocity which accounts only for the turbulence that exists in front of the flame front (Schmid's relation [22]), S_L the laminar burning velocity (function of pressure), Da the Damköhler number, u' is the rms (root mean square) of velocity fluctuations and Ξ are factors that account for the various mechanisms which accelerate the combustion process. The above formulation of the combustion model considers that the modelled phenomena are independent from each other and thus to wrinkle the flame at different scales [20]. We should note that as u' goes to zero, S_T goes to $S_L^{sgs} = \Xi_k \cdot \Xi_{lp} \cdot \Xi_{T_0} \cdot S_L$

Ξ_k accounts for turbulence that is generated by the flame front itself. This phenomenon is driven by the hydrodynamic instability, and as a result Ξ_k depends on the expansion coefficient E. Hydrodynamic instability needs some distance, R_0 , in order to be fully developed. In order to account for the transient stage, Ξ_k is estimated from the relation $\Xi_k = 1 + \left(\psi \cdot \Xi_k^{\max} - 1\right) \cdot \left[1 - \exp\left(-R/R_0\right)\right]$ [23][24] where R is the distance from the ignition point and $\Xi_k^{\max} = \left(E - 1\right)/\sqrt{3}$ [25]. ψ is a model constant varying between 0 and 1 which represents the level at which the maximum value $\Xi_k^{\max}$ is reached.

Ξ_{lp} accounts for non-equidiffusive effects. In lean hydrogen mixtures, non-equidiffusive effects make the flame unstable wrinkling its surface and increasing the combustion rate [26]. This instability, which is often called diffusional-thermal, develops faster than the hydrodynamic one and thus it influences the deflagration process at the very early stages [27]. Ξ_{lp} increases linearly from the value of one to a constant maximum value at a given distance where the instability is considered to be fully developed. This distance is set equal to 0.1 m based on the experimental data of Kim et al. (2015) [27]. The maximum value of Ξ_{lp} can be estimated [28] based on the leading point concept of Zimont and Lipatnikov work [29]. For 18% hydrogen concentration, it is approximately equal to 2. This is in agreement with the value of 1.96 which can be estimated from the experiments of Bauwens et al. (2011) [8]. The value of 1.96 was used in this study for both 15 and 18% mixture concentration. The fact that the effect of diffusional-thermal instability can be modelled by increasing the burning velocity by a constant factor is supported by the work of Bauwens et al. [12][8].

Compared to the model developed in [20], the coefficient Ξ_{T_0} has been added in this study in order to take into account the effect of initial turbulence. It is a constant value which is applied everywhere in

the domain. Its value is greater than 1 only for the cases with significant levels of initial turbulence, i.e. the FM-Global 15% concentration cases with u' equal to 0.4 and 0.5 m/s. Bauwens et al. (2014) [12] suggests this modelling practice based on their observations of the initial turbulence effect on the flame speed. They modified their analytical model for vent sizing and reasonable agreement with the experiment was found. In CFD simulation, the effect of initial turbulence could be accounted for with proper initial values of k and ε. However, simulation results depend strongly on the initial values of ε which were not measured during the experiments. Consequently, we take into account the initial turbulence as it is suggested in [12] and we use very low initial values of k and ε (equal to 1.0e-06 m^2/s^2 and 1.0e-06 m^2/s^3 respectively for all cases). In this way, the validity of the approach suggested in [12] is evaluated for CFD modelling.

The values of the main parameters of the model are presented in Table 1. Laminar flame speed at initial pressure, S_{L0}, and expansion coefficient, depend only on mixture composition. The parameters for the estimation of the Ξ_k coefficient, R_0 and ψ, were chosen based on guidelines [24][30] and in order to match the experimental overpressure at the initial stages of the back ignition deflagration cases. This means that for a given experimental set-up the same parameters are used in the back and center ignition case. Regarding R_0, guidelines [30] suggest maximum value equal to 1.2 m for hydrogen mixtures. This value is proposed to be decreased for lean mixtures where the transition to turbulence is expected to occur quicker. Lower values are expected also if initial turbulence exists. As a result, in our cases, R_0 equal to 1.0 m is used in KIT experiment where near zero values of initial turbulence exists, 0.8 m in 18% FM-Global cases where small initial turbulence exists and 0.3 m in 15% FM-Global cases where higher values exist. The value of ψ is set equal to 1.0 except from the two FM-Global cases with 18% hydrogen concentration for which the value of 0.9 is chosen.

Table 1. Main model parameters for each experimental case

Experimental cases					**Modelling parameters**				
No	Experiment	Conc. (v/v)	Ignition	Initial u' (m/s)	S_{L0} (m/s)	E	R_0 (m)	ψ	Ξ_{T_0}
1	KIT	18%	Back	-	0.64	5.20	1.0	1.0	1.00
2	FM-Global	18%	Back	~ 0.1	0.64	5.20	0.8	0.9	1.00
3	FM-Global	18%	Center	~ 0.1	0.64	5.20	0.8	0.9	1.00
4	FM-Global	15%	Back	0.12	0.38	4.68	0.3	1.0	1.00
5	FM-Global	15%	Back	0.40	0.38	4.68	0.3	1.0	1.12
6	FM-Global	15%	Back	0.50	0.38	4.68	0.3	1.0	1.17
7	FM-Global	15%	Center	0.12	0.38	4.68	0.3	1.0	1.00
8	FM-Global	15%	Center	0.40	0.38	4.68	0.3	1.0	1.12
9	FM-Global	15%	Center	0.50	0.38	4.68	0.3	1.0	1.17

3.2 Numerical details

In KIT experiment, computational domain (Figure 4) includes the interior of the room where the vented enclose resides. No-slip boundary conditions were used in all solid boundaries and standard wall functions were applied. Three computational grids were used in order to assess grid independence, a coarse one with approximately 714,000 cells, a medium one with 1,539,000 cells and a fine one with 2,726,000 cells. The control volumes size was approximately uniform inside the enclosure and outside until the distance of 0.8 m from the vent and equal to 0.03, 0.02 and 0.015 m for the coarse, medium and fine grid respectively. The expansion ratio outside that uniform region was set equal to 1.08. The results exhibit small grid dependency [20] and the ones of the fine grid are presented in Section 4.0.

In FM-Global experiments, symmetry in the y axis was assumed. The domain covers the area from -10 m to 40 m in the horizontal direction and from 0 m to 30 m in the lateral and vertical direction. The center of the room was placed at the origin of the coordinate system. Symmetry boundary conditions were applied in the south plane of the domain and non-reflecting boundary conditions in all other open boundary planes. Two computational grids were examined, a coarse one with approximately 395,560, cells and a fine one with 893,412 cell. The control volumes size was approximately uniform inside the enclosure and outside until the distance of 4.2 m from the vent and equal to 0.075 and 0.01 m for the coarse and fine grid respectively. The maximum expansion ratio outside that uniform region was equal to 1.1. The results from the grid independency study are presented in Section 4.0.

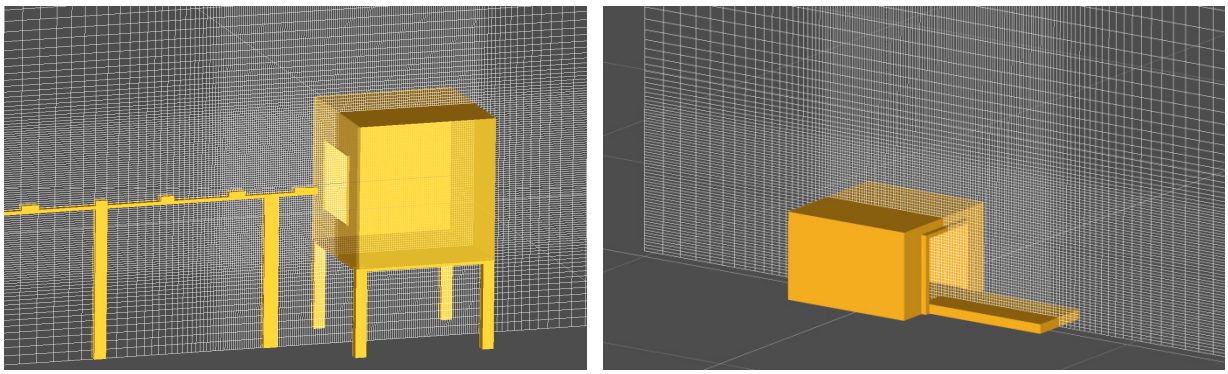

Figure 4. Geometry and part of the domain for the KIT (left) and the FM-Global (right) experiments. The fine grid in XZ plane passing through the center of the enclosures (symmetry plane in the FM-Global case) is also shown.

ADREA-HF uses the finite volume method on a staggered Cartesian grid. The pressure and velocity equations are decoupled using a modification of the SIMPLER algorithm. For the discretization of the convective terms the bounded second order upwind method is used [31]. For time advancement, the fully implicit first order accurate scheme was chosen. Time step is automatically adapted according to desired Courant–Friedrichs–Lewy (CFL) number which was set equal to 0.2. Smaller CFL numbers were examined and no differences in the results were found. As initial conditions, a stagnant flow field with no turbulence is specified. Ignition is modelled by fixing the reaction rate in a cell at the ignition point, in order the initial amount of fuel to be burned at a determined interval estimated by the formula $0.5dx/\left(E \cdot S_{L0}\right)$ where dx is the size of the cell at ignition point.

4.0 RESULTS AND DISCUSSION

4.1 Simulation of KIT experiments

A thorough analysis of the simulation results for this experiment can be found in [20]. In this study, only the main results are presented for comparison with the FM-Global simulations. In Figure 5 (left) the simulation results for the overpressure inside and outside the enclosure are compared against experimental results. We observe that the CFD model achieves very good agreement with the experiment. At the initial stage of deflagration when the flame is inside the enclosure the agreement is excellent in both internal and external overpressure. When the flame exits the vent (0.077 s) the pressure inside the enclosure stabilises around 5.8 kPa, similarly to the experiment. The time when pressure increases inside and outside the enclosure due to external explosion is also predicted very accurately. The rate of pressure increase inside the enclosure is captured very well. However, the maximum overpressure is overpredicted by approximately 17%.

In Figure 5 (right) the predictions of combustion related parameters, i.e. turbulent burning velocity S_T , rms velocity fluctuations u' and $S_L^{sgs} = \Xi_k \cdot \Xi_{lp} \cdot \Xi_{T_0} \cdot S_L$ are presented for the flame inside or outside the enclosure. These are the mean values of the variables at the flame front that exists only inside or

outside the enclosure. We observe that inside the enclosure the effect of turbulence existing in front of the flame front on combustion (which is expressed through u') is minor. As a result flame instabilities are responsible for the increase of the reaction rate inside the enclosure. Outside the enclosure the effect of turbulence gets bigger which leads to the deviation of S_T from S_L^{sgs}.

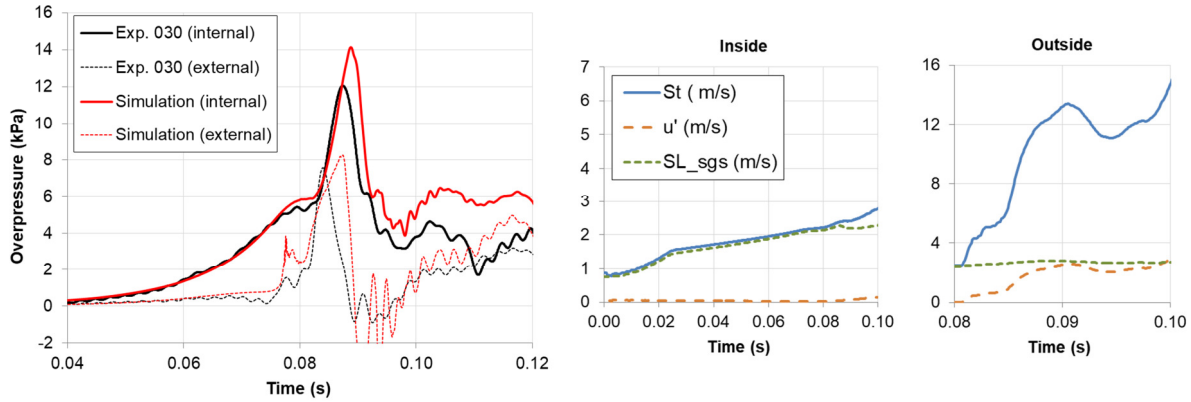

Figure 5. KIT experiment. Left: Overpressure inside and outside the enclosure. Right: Average predicted combustion related variables at the flame front inside or outside the enclosure.

In Figure 6 (left) the hydrogen mass fraction isosurface along with the flame front surface are presented at the onset of the external pressure sudden increase (0.081 s). In the same diagrams the contours of u' are shown at the central xz plane along with the velocity vectors. We observe that at this time the flame enters the area of high turbulence which has been formed lateral of the vent edges. Thus, the reaction rate increases and the pressure rises. In the same figure (at the right) photo of the experiment at the same time is presented where both the hydrogen cloud which has been pushed outside the vent and the flame can be seen. The agreement with the experiment regarding the general shape and position is very satisfactory.

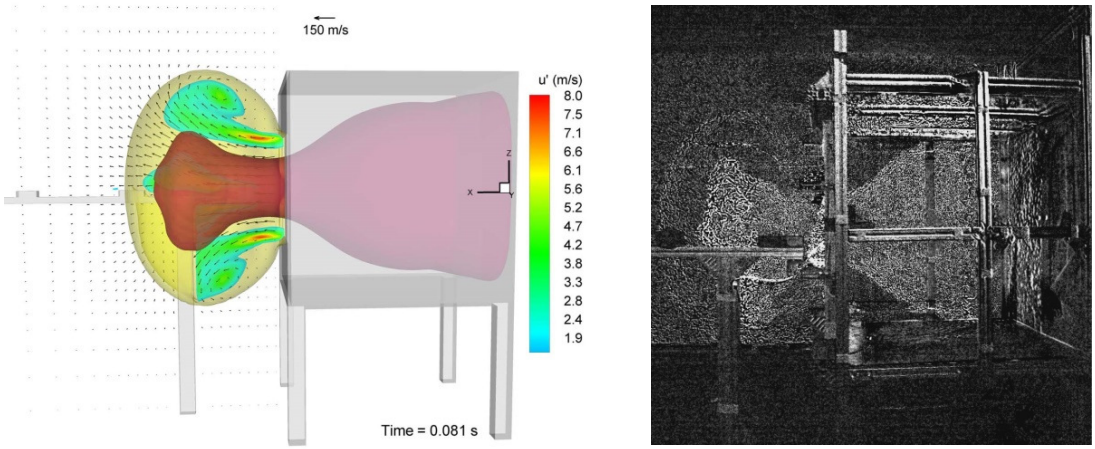

Figure 6. KIT experiment. Left: Hydrogen mass fraction isosurface (yellow) and flame front surface (dark red) along with u' contours (cutoff below 1.5 m/s) and velocity vectors at the onset of external pressure sudden increase (0.081 s). Right: Photos of the experiment at the same time.

4.2 Simulations of FM-Global experiments

In Figure 7 (left) the simulation results for the overpressure inside and outside the enclosure are compared against experimental measurements. The maximum internal overpressure is underestimated by approximately 14% whereas the maximum external overpressure is predicted almost perfectly by both grids. The only significant difference between the examined grids is that in the fine grid case the overpressure remains approximately steady at the period 0.235-0.250 s whereas in the coarse grid case

the pressure continuously increases. However, the noticeable pressure drop in the experiment at the same period of time is not reproduced in both grids.

In Figure 7 (right) the predictions of combustion related parameters are presented for the flame inside or outside the enclosure. We observe that, similarly to the KIT case (Section 4.1), the effect of turbulence existing in front of the flame front on combustion is minor inside the enclosure whereas it is the dominant one outside the vent at the time when external explosion occurs.

In Figure 8, u' contours are presented along with the flame front at two times. The outer limit of the area that is occupied by the hydrogen which has been pushed outside the enclosure is also shown. The first picture corresponds to the time when the internal overpressure has been stabilized (external pressure equal to 2.84 kPa at that time) whereas the second one at the onset of internal pressure sudden increase. The external pressure increase has begun in the second picture and it is equal to 4.8 kPa at that specific time. We observe that, similarly to the KIT case, the high turbulence area that has been generated outside the enclosure is responsible for the flame acceleration and the violence of the external explosion. The high turbulence area develops mainly away from the centreline of the opening at the areas of recirculation. This also holds for the XY planes not shown here in which u' contours have similar shape.

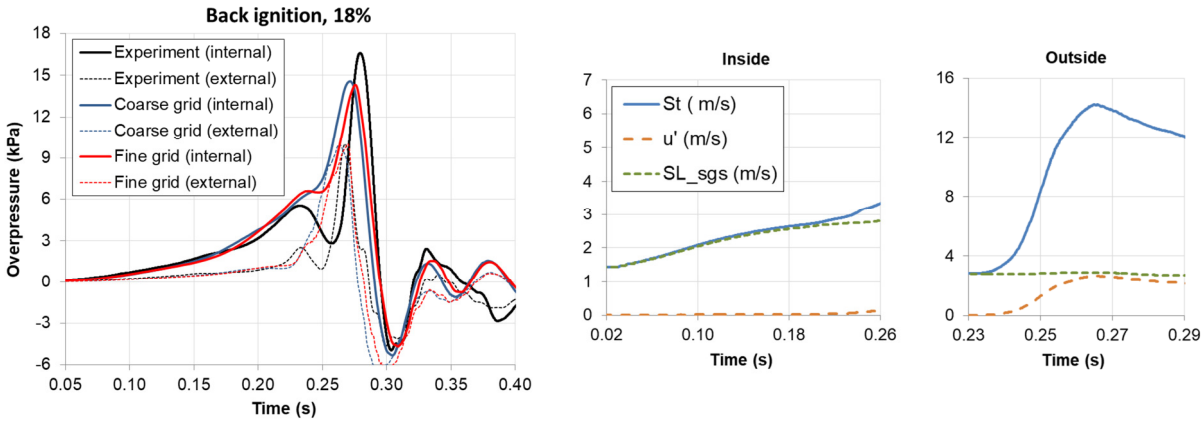

Figure 7. Back ignition case, 18% v/v hydrogen concentration. Left: Overpressure inside and outside the enclosure. Right: Average predicted combustion related variables at the flame front inside or outside the enclosure for the fine grid simulation.

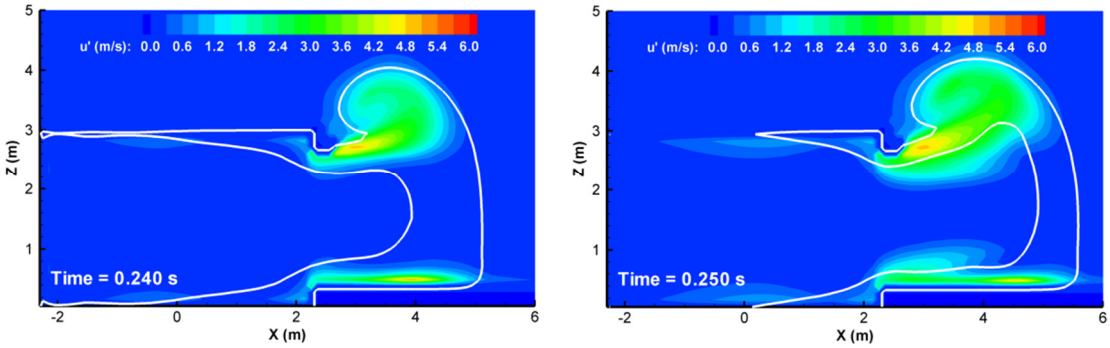

Figure 8. Back ignition case, 18% v/v hydrogen concentration. u' contours along with the flame front (inner white curve) and the outer limit of hydrogen cloud (outer white curve) at the symmetry plane.

In Figure 9 (left) the results from the central ignition case are presented. We observe that the two grids give almost identical results. Comparing with the experiment, the maximum external overpressure is overpredicted by approximately 32% which is caused by the overprediction of the external pressure. At the initial phase of deflagration, a time delay in the simulation results exists compared to the experiment. In Figure 9 (right) the predictions of combustion related parameters are presented. The

model behaviour is similar to the one of the previous cases. Flame instabilities are responsible for the flame acceleration when the flame is inside the enclosure whereas turbulence is responsible for the external explosion.

In Figure 10, u' contours are presented along with the flame front and the hydrogen cloud. The time 0.19 s corresponds to the time when the pressure inside the enclosure has been stabilized whereas the time 0.20 s corresponds to the time when the pressure increase has begun. Similarly to the back ignition case, pressure increases rapidly when the flame enters the high turbulence area that has been formed around the vent.

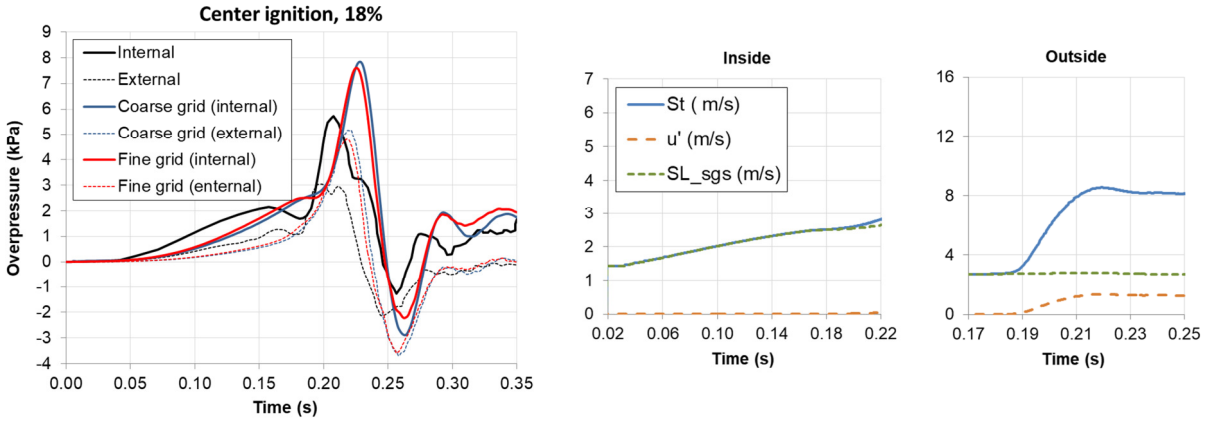

Figure 9. Center ignition case, 18% v/v hydrogen concentration. Left: Overpressure inside and outside the enclosure. Right: Average predicted combustion related variables at the flame front inside or outside the enclosure for the fine grid simulation.

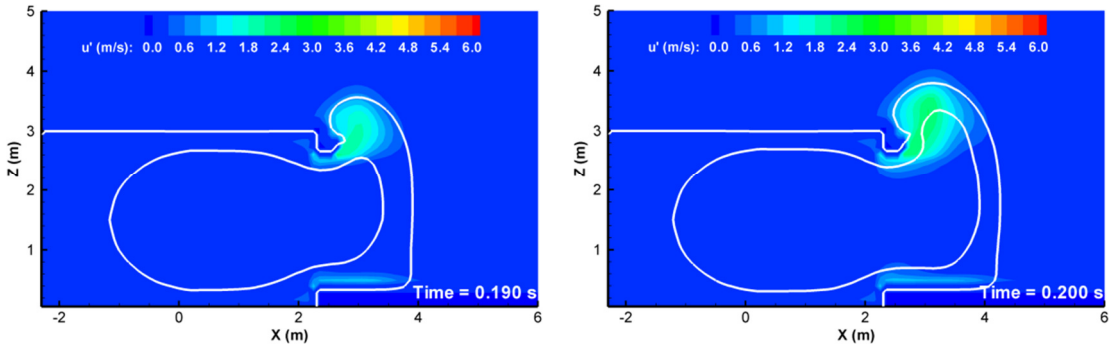

Figure 10. Center ignition case, 18% v/v hydrogen concentration. u' contours along with the flame front (inner white curve) and the outer limit of hydrogen cloud (outer white curve)

Figure 11 presents the overpressure time series for the 15% hydrogen concentration cases and back-wall ignition for various levels of initial turbulence. Grid independency was performed in these cases too and grid convergence was very satisfactory, similar to the one presented for the 18% cases. We observe that the agreement with the experiment is very good in all cases. Maximum overpressure is captured almost perfectly with maximum relative error being equal to 6%. The qualitative features of the time series are also predicted very well. The local maximum at the time when the flame exits the vent (e.g. at 0.33 s for the $u' = 0.50$ m/s case) is reproduced by the simulations, as well as the local minimum which follows. The value of this minimum, however, is overpredicted in all cases.

In Figure 12, the results for the center ignition case are presented. We observe that the model overpredicts the maximum overpressure in all cases. The overprediction is equal to 54, 61 and 30% for u' equal to 0.12, 0.40 and 0.50 m/s respectively. The deviations from the experiments in the central ignition cases are likely to be partially caused by the omission of a vent cover opening model. In central ignition case, the flame is closer to the vent at the time of the vent opening and thus the results

can be influenced in a greater extent compared to the back ignition case. This is evident in the experimental overpressure time series, as we comment in Section 2.2.

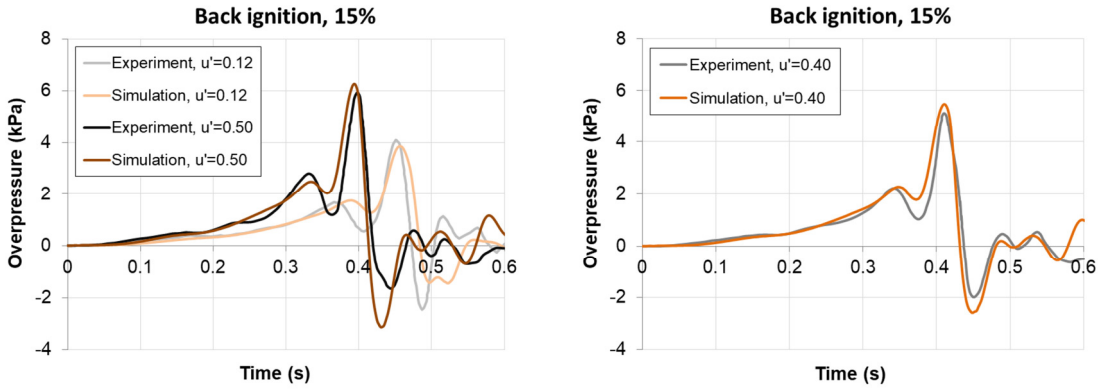

Figure 11. Back ignition case, 15% v/v hydrogen concentration. Overpressure time series for various values of initial turbulence. Comparison between simulation and experimental results.

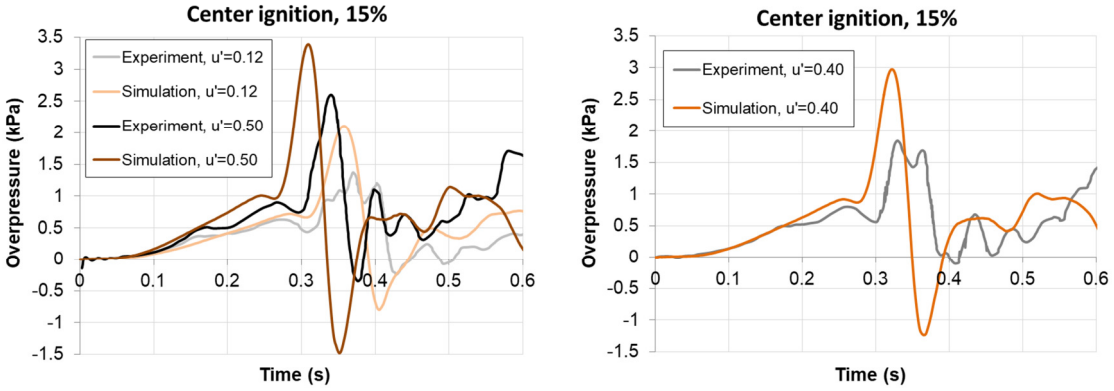

Figure 12. Center ignition case, 15% v/v hydrogen concentration. Overpressure time series for various values of initial turbulence. Comparison between simulation and experimental results.

5.0 CONCLUSIONS

A newly developed CFD model for vented deflagration simulations was evaluated against nine experimental cases. The model exhibited very good performance for the back ignition cases. The maximum deviation from the experiments of the maximum overpressure was equal to 17% in those cases. The model reproduced successfully all the qualitative features of the overpressure curves with only exception the local minimum before external explosion in FM-Global 18% case. In central ignition cases, the model overpredicted the maximum overpressure up to 61%. However, study of the experimental results indicates that the opening of the vent cover may have a significant impact on the result in these cases. No model for vent opening was considered in this study.

Regarding the effect of initial turbulence, this was reproduced successfully by applying only a constant factor in the burning velocity. This is in agreement with the finding of experimentalists. The value of this constant is small being equal to 1.17 for u' equal to 0.50 m/s case.

Regarding the physics of the phenomenon, the results indicate that flame instabilities are primarily responsible for the acceleration of the flame front while it is inside the enclosure. Turbulence in front of the flame front mainly develops outside the vent at the recirculation areas leading the significant increase of pressure when the flame enters this area.

ACKNOWLEDGEMENTS

This Publication is supported by the program of Industrial Scholarships of Stavros Niarchos Foundation, Greece. The authors would like to gratefully thank Dr. Regis Bauwens for providing experimental data for the FM-Global experiments.

REFERENCES

[1] Chao J, Bauwens CR, Dorofeev SB. An analysis of peak overpressures in vented gaseous explosions. Proc Combust Inst 2011;33:2367–74. doi:10.1016/j.proci.2010.06.144.

[2] Harrison AJ, Eyre JA. External Explosions as a Result of Explosion Venting. Combust Sci Technol 1987;52:91–106. doi:10.1080/00102208708952570.

[3] Jiang X, Fan B, Ye J, Dong G. Experimental investigations on the external pressure during venting. J Loss Prev Process Ind 2005;18:21–6.

[4] Proust C, Leprette E. The dynamics of vented gas explosions. Process Saf Prog 2010;29:231–5. doi:10.1002/prs.10368.

[5] Molkov VV, Makarov DV. Rethinking the Physics of a Large-Scale Vented Explosion and its Mitigation. Process Saf Environ Prot 2006;84:33–9. doi:10.1205/psep.04232.

[6] Molkov V, Makarov D, Puttock J. The nature and large eddy simulation of coherent deflagrations in a vented enclosure-atmosphere system. J Loss Prev Process Ind 2006;19:121–9. doi:10.1016/j.jlp.2005.05.006.

[7] Makarov D, Verbecke F, Molkov V. Numerical analysis of hydrogen deflagration mitigation by venting through a duct. J Loss Prev Process Ind 2007;20:433–8. doi:10.1016/j.jlp.2007.04.022.

[8] Bauwens CR, Chaffee J, Dorofeev SB. Vented explosion overpressures from combustion of hydrogen and hydrocarbon mixtures. Int J Hydrogen Energy 2011;36:2329–36. doi:10.1016/j.ijhydene.2010.04.005.

[9] Keenan JJ, Makarov DV, Molkov VV. Rayleigh–Taylor instability: Modelling and effect on coherent deflagrations. Int J Hydrogen Energy 2014;39:20467–73. doi:10.1016/j.ijhydene.2014.03.230.

[10] Kuznetsov M, Friedrich A, Stern G, Kotchourko N, Jallais S, L'Hostis B. Medium-scale experiments on vented hydrogen deflagration. J Loss Prev Process Ind 2015;36:416–28. doi:10.1016/j.jlp.2015.04.013.

[11] HyIndoor, Pre normative research on the indoor use of fuel cells and hydrogen systems, Work Package 3: Vented Deflagrations, D3.4: Final report on analytical, numerical and experimental studies of hydrogen vented deflagrations 2014.

[12] Bauwens CR, Dorofeev SB. Effect of initial turbulence on vented explosion overpressures from lean hydrogen–air deflagrations. Int J Hydrogen Energy 2014;39:20509–15. doi:10.1016/j.ijhydene.2014.04.118.

[13] Bauwens CR, Chao J, Dorofeev SB. Effect of hydrogen concentration on vented explosion overpressures from lean hydrogen–air deflagrations. Int J Hydrogen Energy 2012;37:17599–605. doi:10.1016/j.ijhydene.2012.04.053.

[14] Bauwens C, Chaffee J, Dorofeev S. Experimental and numerical study of hydrogen–air deflagrations in a vented enclosure. 7th Int. Symp. hyzards Prev. Mitig. Ind. Explos., St. Petersburg, Russia: 2008.

[15] Bauwens C, Chaffee J, Dorofeev S. Vented explosion overpressures from combustion of hydrogen and hydrocarbon mixtures. 3th Int. Conf. Hydrog. Saf., Ajaccio, France: 2009.

[16] Bauwens CR, Dorofeev SB. Hydrogen Vented Deflagrations at FM Global: Tests and Modeling. Presentation in "Advanced Research Workshop: Progress in safe indoor use of fuel cells and hydrogen systems", September 12th 2013.

[17] Venetsanos AG, Papanikolaou EA, Bartzis JG. The ADREA-HF CFD code for consequence

assessment of hydrogen applications. Int J Hydrogen Energy 2010;35:3908–18. doi:https://doi.org/10.1016/j.ijhydene.2010.01.002.

[18] Tolias IC, Venetsanos AG, Markatos N, Kiranoudis CT. CFD modeling of hydrogen deflagration in a tunnel. Int J Hydrogen Energy 2014;39:20538–46. doi:10.1016/j.ijhydene.2014.03.232.

[19] Kato M, Launder BE. The modeling of turbulent flow around stationary and vibrating square cylinders. Ninth Symp. Turbul. Shear Flows, Kyoto, Japan, August 16-18: 1993.

[20] Tolias IC, Venetsanos AG. An improved CFD model for vented deflagration simulations – Analysis of a medium-scale hydrogen experiment. Int J Hydrogen Energy 2018;43:23568–84. doi:10.1016/J.IJHYDENE.2018.10.077.

[21] Lipatnikov AN, Chomiak J. Turbulent flame speed and thickness: phenomenology, evaluation, and application in multi-dimensional simulations. Prog Energy Combust Sci 2002;28:1–74.

[22] Schmid H-P, Habisreuther P, Leuckel W. A Model for Calculating Heat Release in Premixed Turbulent Flames. Combust Flame 1998;113:79–91. doi:10.1016/S0010-2180(97)00193-4.

[23] Molkov V, Makarov D, Schneider H. LES modelling of an unconfined large-scale hydrogen-air deflagration. J Phys D (Applied Physics) 2006;39:4366–76. doi:10.1088/0022-3727/39/20/012.

[24] Xiao H, Makarov D, Sun J, Molkov V. Experimental and numerical investigation of premixed flame propagation with distorted tulip shape in a closed duct. Combust Flame 2012;159:1523–38. doi:10.1016/j.combustflame.2011.12.003.

[25] Karlovitz B, Denniston DW, Wells FE. Investigation of Turbulent Flames. J Chem Phys 1951;19:541. doi:10.1063/1.1748289.

[26] Jomaas G, Law CK, Bechtold JK. On transition to cellularity in expanding spherical flames. J Fluid Mech 2007;583:1–26. doi:10.1017/S0022112007005885.

[27] Kim WK, Mogi T, Kuwana K, Dobashi R. Self-similar propagation of expanding spherical flames in large scale gas explosions. Proc Combust Inst 2015;35:2051–8. doi:10.1016/j.proci.2014.08.023.

[28] Molkov V. Fundamentals of Hydrogen Safety Engineering, parts I & II. Free download e-book, bookboon.com, ISBN: 978-87-403-0279-0; 2012.

[29] Zimont V, Lipatnikov A. A numerical model of premixed turbulent combustion of gases. Chem Phys Rep 1995;14:993–1025.

[30] Molkov V, Bragin M. Hydrogen–air deflagrations: Vent sizing correlation for low-strength equipment and buildings. Int J Hydrogen Energy 2015;40:1256–66. doi:10.1016/j.ijhydene.2014.11.067.

[31] Waterson NP, Deconinck H. Design principles for bounded higher-order convection schemes – a unified approach. J Comput Phys 2007;224:182–207. doi:https://doi.org/10.1016/j.jcp.2007.01.021.